Hydrodynamic Behavior of Circulating Fluidized Bed with Polymeric Particles

Peijun Jiang, Hsiaotao Bi, Shu-Chien Liang, and Liang-Shih Fan
Dept. of Chemical Engineering, The Ohio State University, Columbus, OH 43210

A systematic study conducted explores the hydrodynamics of a circulating fluidized bed with polymeric particles employing polyethylene resins with a particle density of 660 kg/m^3 and size ranging from 90 to 500 μm. The study indicates that polyethylene resins can be fluidized smoothly in the fast fluidization regime. However, the operating range of the fast fluidization regime for these particles is smaller than that for FCC particles. The deviation of the fluidization behavior of polyethylene particles from that of common Group-A particles is explained considering the interparticle forces. Experiments with fine polyethylene particles are also conducted with coarse particles added in a circulating fluidized bed. Axial profiles of solid holdups in a bed with and without coarse particles, as well as overall fine particle holdup, are studied. The results show a significantly wider operating range of the fast fluidization regime and enhancement of fine particle holdups in a bed with the presence of coarse particles. For comparison, fluidization with FCC particles is also conducted. A mechanistic model considering particle-particle collision is proposed. The model accounts for the momentum exchange rate between a coarse particle and a cloud of fine particles, which explains the enhancement of fine particle holdups observed experimentally.

Introduction

Fluidized beds have been commonly employed in industry for polymerization reactions (Kunii and Levenspiel, 1991), and most are conducted under the bubbling or turbulent fluidization regimes. Although no commercial circulating fluidized-bed reactor for polymerization exists, a study of hydrodynamic behavior is warranted from a fundamental standpoint, which is concerned with the hydrodynamic behavior of polymeric particles in a circulating fluidized bed. These particles are polyethylene resins which are of low density, low hardness and rough surface. For comparison of hydrodynamic behavior, experiments using FCC particles in a circulating fluidized bed are also conducted. The analysis of the fluidization behavior is made by considering the interparticle forces. Fluidization of fine particles in a circulating fluidized bed is also studied for the conditions with addition of coarse particles, and their effects are examined.

Extensive hydrodynamics studies of circulating fluidized beds have been reported in the literature (for example, Basu, 1986; Large and Basu, 1988; Basu et al., 1990). However, relatively little work has been conducted concerning the particle physical property effects, particularly the particle density effects on the hydrodynamics of the system. Weinstein et al. (1984) and Bi (1988) studied a circulating fluidized bed with particles of different densities and found the axial variation of solids holdups to be much smaller for lighter particles than for heavier particles. A similar trend was also reported by Li et al. (1990) in the study of low density aerogel powders in a small-scale circulating fluidized bed. Using particles with different surface friction coefficients, Chang and Louge (1992) found that particles with smaller surface friction coefficients yield a smaller pressure drop. Little is known regarding the hydrodynamic behavior of a circulating fluidized bed with polymer resin particles.

A distinctive property of polymeric particles (such as polyethylene resin particles), which affects their transport behavior, is the dielectric characteristics. When two particles are in contact, movement of electric charges occur through their boundary surface leading to a formation of a double electric

Correspondence concerning this article should be addressed to L.-S. Fan.

layer along the boundary surface in which positively charged elements prevail on one side, and negatively charged elements prevail on the other. On the other hand, when the two particles are separated, the charges which have been displaced do not undergo recombination or neutralization leading to electrically charged particles. Cartwright et al. (1982) reported that when relatively dry polyethylene particles were introduced into a conveying loop, bipolar charging occurred and coarse particles were charged positively. The charge accumulation on particles of dielectric materials in fluidized beds was also reported by Wolny and Kazmierczak (1989) and Wolny and Opalinski (1983). Their results suggested that both positively and negatively charged particles exist in the fluidized bed. In the circulating fluidized bed, triboelectrification caused by particle-particle contact, as well as particle-wall contact, can have a profound effect on the flow behavior of the particles. Increased pressure drops in pneumatic transport systems have been reported by Smeltzer et al. (1982). Richardson and McLeman (1960) attributed the increase in pressure drop and relative velocity between particles and fluid to the electrostatic attraction between the dust layer left on the wall and the main body of the particles. Little is known regarding the effects of the electrostatic charge of polymer particles on the hydrodynamic behavior of a circulating fluidized bed.

Strong interparticle forces of polyethylene resins could induce particles to form agglomerates. However, with the addition of coarse particles it may be possible to suppress much of the agglomeration through fine and coarse particle interactions. In a previous article (Bi et al., 1992), it was demonstrated that in the circulating fluidized bed of fine particles (FCC), with an addition of large glass beads (GB), solids holdup can be significantly enhanced. It was also reported that the hydrodynamic behavior for a bed with mixed particles of a wide size distribution is different from that with particles of a narrow size distribution. For example, particle segregation occurs in a pneumatic transport system (Nakamura and Capes, 1976) and a circulating fluidized bed (Ijichi et al., 1990) with nonuniform particle properties. Geldart and Pope (1983) reported that the significant interactions between fast-moving fine particles and slow moving coarse particles could yield a profound increase in the carryover of coarse particles in the freeboard of a fluidized bed. Furthermore, Bagster and Roberts (1985) and Li et al. (1990) reported that the mobility or fluidization quality of fine powders was affected by adding or removing large particles from a high velocity fluidized bed.

Experimental Studies

A schematic diagram of the circulating fluidized bed used in this study is shown in Figure 1. It consists of a riser of 102 mm ID and 6.32 m height, a separator and a secondary cyclone system, an L-valve and a large particle storage hopper. All the parts except the separator are made of Plexiglas. The particles are carried upwards through the riser and exit at the top through a right angle bend into a 102 mm diameter horizontal tube connected to the separator. The particles are separated from the gas by the separator and the secondary cyclone at the top of the riser, and fed back to the riser through the L-valve located at the bottom of the riser. The solids circulation rate is controlled by adjusting the air flow rate at the injection points of the L-valve. The solids circulation rate is measured

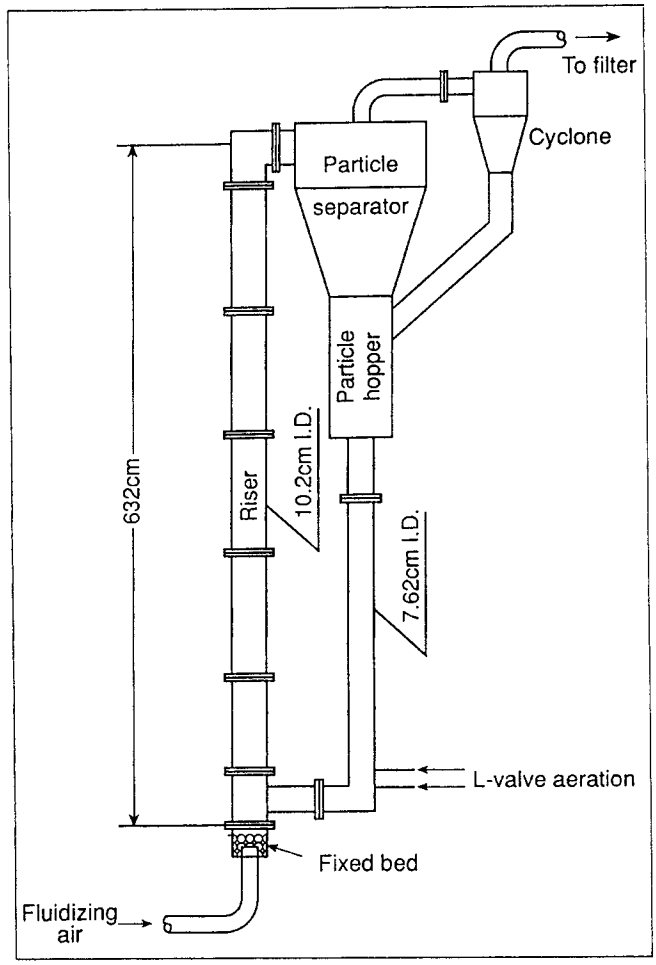

Figure 1. Circulating fluidized bed.

by timing the descent distance of identifiable particles in the standpipe. In the absence of coarse particles, the cross-sectional averaged bed voidages are obtained from the pressure profiles. An optic fiber probe, which is calibrated using the method employed by Zhang et al. (1991), is used to measure local solids concentration. The relative humidity of the air, which is monitored by a psychrometer, is maintained at about 14%.

There are 18 pressure taps along the riser and the distance between two adjacent pressure taps varies within the range of 150–400 mm. Pressures along the riser are measured using manometers. Differential pressure transducers with high sensitivity and frequency response (100 Hz) are connected to the pressure taps, which are flush mounted on the inner wall of the riser. The length of connecting tubes is also kept short to minimize the signal damping. The dead volumes of connecting tubes and the chamber inside the DP cell on either side of the differential transducer are kept equal (Clark and Atkinson, 1988) for accurate differential pressure measurement. Analog outputs of the transducers are interfaced with a microcomputer data acquisition system for data collection, with a sampling rate of 50 Hz.

The fine particles used are polyethylene resins (PE) and FCC particles, and both belong to Geldart's Group A. The coarse particles used in the experiments are 4.4 mm polyethylene spheres (CPE) and 2 mm GB. The physical properties of the particles along with the particle terminal velocities and the

Table 1. Properties of Particles

Particles	d_p (μm)	ρ_b (kg/m^3)	ρ_s (kg/m^3)	U_t (m/s)	U_{mf} (ms)	Permittivity	Resistivity (Ωm)
FCC	89	793	1,153	0.27	0.0044	n/a	n/a
Polyethylene Resin (PE)	325	445	660	1.32	0.027	2.3 (60 Hz)	10^{18}
Polyethylene (CPE)	4,400	664	1,010	10.70	4.67	2.3 (60 Hz)	$>10^{13}$
Glass Beads (GB)	2,000	1,559	2,500	11.30	2.61	12.1 (1 kHz)	2×10^{11}

incipient fluidization velocities evaluated from correlations are given in Table 1. To evaluate the relative importance of various forces exerted on particles, information on dielectric properties (particle resistivity and permittivity) is also given in Table 1. The extent of redistribution of the electric charges transferred at particle contact points depends on the product of permittivity and resistivity. SEM graphs of polyethylene particles in Figure 2 show the surface characteristics of the PE particles which are of nodular surface and irregular shape.

In the experiments with coarse particles, the coarse particles are introduced to the bed before starting the run. The gas velocities used are higher than the transport velocity of fine particles, but lower than the terminal velocity of the coarse particles. Thus, when the bed consists of coarse particles only, the particles are not carried over by the gas. Under low solids circulation rates, the coarse particles are all retained in the bed without being recirculated. However, under high solids circulation rates, these particles are carried over and circulated with the fine particles. Note that when the coarse particles are recirculated with the fine particles, the extent of the solids circulation rate reported here represents that for the fine-coarse particles mixture.

Results and Discussion

Operating regimes

A plot of pressure drop ($-\Delta P/\Delta L$), measured at the bottom section of the bed, vs. solids circulation rate for polyethylene particles is given in Figure 3. It is seen that for gas velocities below the transport velocity, U_{tr}, of 2.2 m/s, there is a sharp increase in the pressure drop across the bottom section with an increase in the solids circulation rate for a given gas velocity. The pressure drop is a direct reflection of the solids holdup in the circulating fluidized-bed systems. For a given gas velocity, a low pressure drop indicates the dilute transport region. As the solids circulation rate increases, a sharp increase in the pressure drop (or solids holdup) takes place at a critical value of the solids circulation rate. When this rate is further increased beyond this critical point, a high solids holdup marks the dense fluidized-bed region. The sharp transition does not exist at gas velocity beyond U_{tr} where the bed is in transport regime. The general ($-\Delta P/\Delta L$) vs. G_s behavior of the polyethylene particles given in Figure 3 is similar to that for FCC particles reported by Yerushalmi et al. (1979). However, the transition from the dilute transport region to the dense fluidized-bed region for the polyethylene particles is not as sharp as that for FCC particles due to the wide particle-size distribution and significant interparticle force effects of the polyethylene particles, which are discussed later.

The operating range of fast fluidization for polyethylene particles can be determined by considering the operational instabilities of the bed and the axial solids holdup profile in the same manner as that reported by Takeuchi et al. (1986). The upper bound of the solids circulation rate for fast fluidization can be determined based on visualization with respect to the bed operational instability at a given gas velocity beyond U_{tr}. There are two types of operational instabilities which are observed in this study. At low gas velocities, choking would occur. At high gas velocities and high solids circulation rates, considerable pressure fluctuation would take place causing considerable amount of the particles in the downcomer to flow into the riser. Thus, the upper bound of the solids circulation rate for fast fluidization, denoted as G_{tf}, at a given gas velocity higher than U_{tr}, is marked by the onset of stable bed operation. The lower bound of the solids circulation rate for fast fluidization can be determined based on uniformity of the axial solids concentration distribution. At a given gas velocity, a decrease in the solids circulation rate will eventually yield a

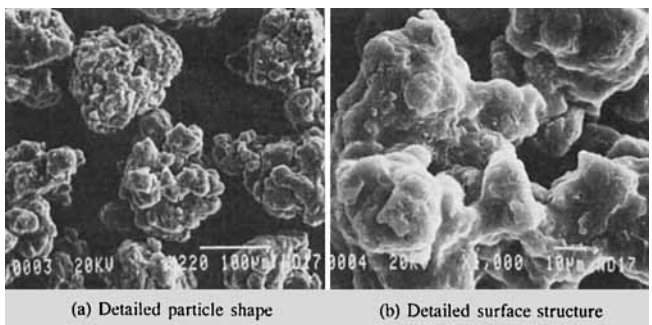

Figure 2. SEM micrograph showing detailed structure of PE particles ($d_p = 137$ μm).

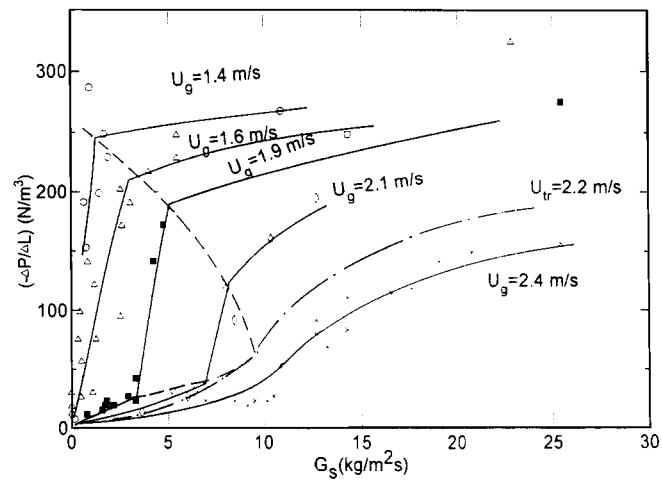

Figure 3. Pressure drop measured at the bottom of the riser as a function of solids circulation rate for polyethylene particles.

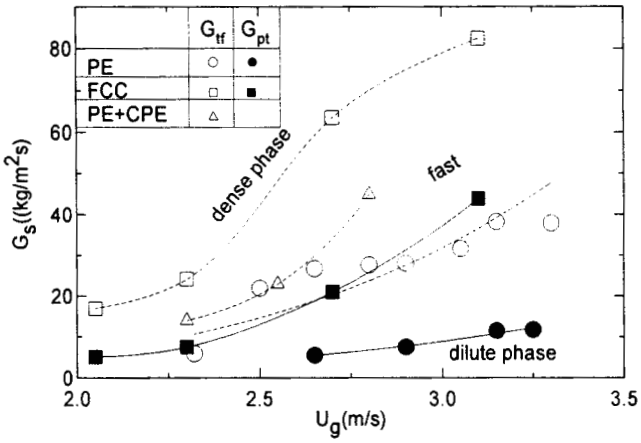

Figure 4. Operating regimes for polyethylene particles (PE) and the PE-CPE mixture.

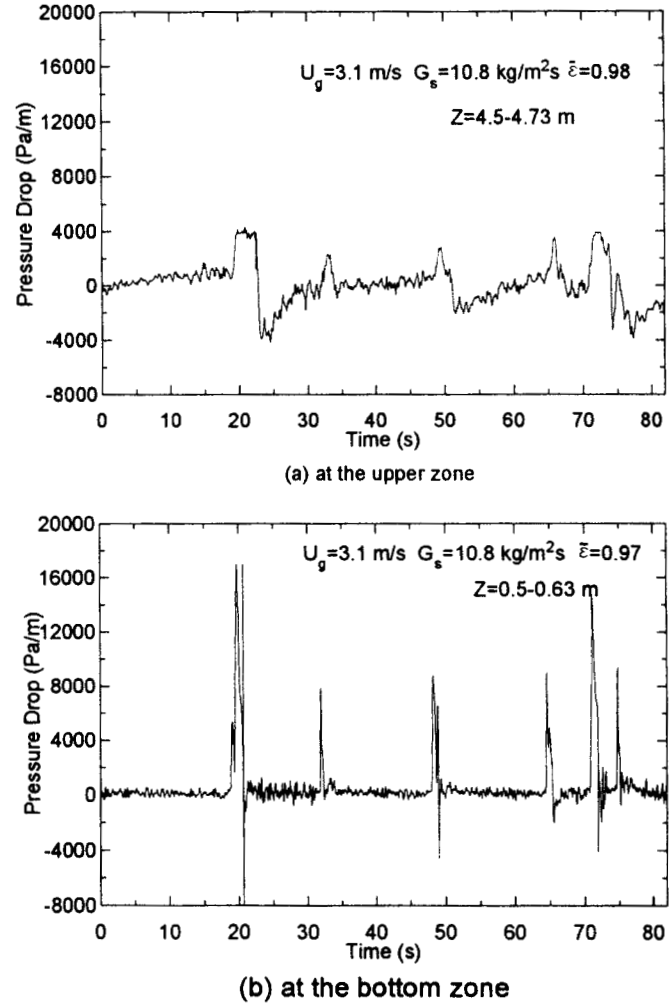

Figure 5. Pressure drop fluctuation measured in the dilute condition.

condition where the axial solids concentration is uniformly distributed. This can also be reflected in the linear profile of the axial pressure distribution. The solids circulation rate which earmarks this condition, denoted as G_{pt}, represents the lower bound of the fast fluidization regime or the onset of the dilute transport regime. Thus, for a given gas velocity, the fast fluidization regime is bounded by G_{tf} and G_{pt}. G_{tf} and G_{pt} curves in terms of the gas velocity vs. solids circulation rate is given in Figure 4 for polyethylene particles. Also shown in the figure are the G_{tf} and G_{pt} for FCC particles. As can be seen in the figure, the operating range of the fast fluidization for the polyethylene particles is not as wide as that for FCC particles.

Although both the PE and the FCC particles employed belong to Geldart's Group A, there is a considerable difference in the bed behavior between FCC particles and polyethylene particles. For the polyethylene particles, when the gas velocity and solids circulation rate are at the lower end of the fast fluidization regime, the solids flow pattern appears to be similar to the immature dune flow observed in a horizontal gas-solid converging system. Particle clusters, with a shape similar to that of small wall-solids-slug observed in the slugging regime, appear in the bed. The cluster in this context refers to a lump of solid particles over which flow properties including voidage do not vary significantly. Note that the particles are in packing state in the L-valve under normal operating conditions. The clusters are formed at the moment when the particles in the L-valve enter the bed. These clusters move as a series of dunes to the exit without being disintegrated; the region not occupied by clusters is dilute in nature. Apparently, the cluster formation is due to interparticle forces including electrostatic forces and van der Waal's forces as all the particles in the cluster are in close association at all times. Violent surges are evidenced in the pressure drop signals, as shown in Figure 5 where pressure drop fluctuations are composed of a number of weak components and very few strong components. The strong components are possibly due to the intermittent passage of the cluster between the pressure taps. Figure 5b shows the fluctuation of the pressure drop signal (ΔP_1) acquired in the lower dense section (z=0.5–0.63 m), while Figure 5a shows the simultaneous measurement (ΔP_2) in the upper dilute section (z=4.5–4.73 m) of the bed. For each peak in the lower section, there is a corresponding peak in the upper section of the bed, implying the passage of the same cluster. Under this operating condition, a slightly unstable operation occurs. Compared with common Group A particles, PE particles are subjected to significant interparticle forces yielding significant deviation in the fluidization behavior. Thus, under relatively low gas velocity and solids circulation rate, the hydrodynamic forces exerted on these particles are not sufficient to overcome the interparticle forces and disintegrate the agglomerates. With an increase in the solids circulation rate, large particle clusters can be broken up by large-scale eddies and a stable operation can be achieved. No similar phenomenon has been observed in the system with high gas velocities and high solids circulation rates.

Solids holdup distributions

Figure 6 shows typical axial bed apparent density profiles for the PE particles. For comparison, the axial profiles obtained for FCC particles are also included in the figure. The gas velocities for polyethylene particles and FCC particles are 2.7 m/s and 1.7 m/s, respectively, yielding a similar particle slip velocity ($\approx U_g/\epsilon - U_t$) for both cases. Comparing Figures 6a and 6b, it can be seen that the axial variations in the solids concentration profiles for the PE particles are smaller compared to FCC particles, although they exhibit a similar trend.

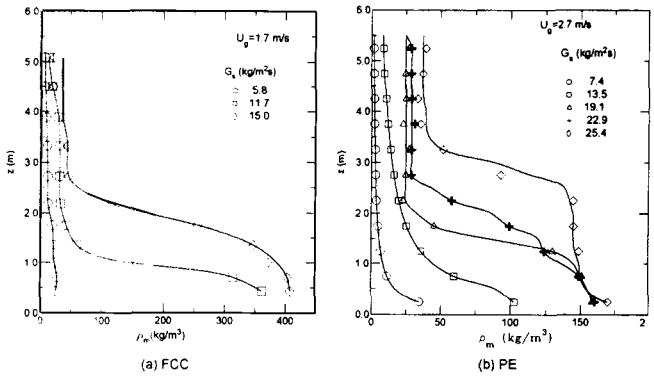

Figure 6. Time-averaged axial distribution of the apparent bed density.

The forces acting on the suspended particles include drag force, buoyancy, gravity and particle interaction forces. The resultant of these forces, characterized by the gas carrying capacity of the particles, appears to be larger for the PE particles than for the FCC particles. The data of the voidage in the bottom dense region for PE particles, however, can be fitted by a simple equation, $\bar{\epsilon} = (U_g + 1)/(U_g + 2)$, proposed by King (1989) for FCC particles.

Time-averaged radial voidage profiles obtained in the lower section of the riser for PE particles are shown in Figure 7 for solids circulation rates of 7.2 and 21.4 kg/m^2·s. For comparison, the results calculated from the correlation proposed by Zhang et al. (1991) are also plotted in the figure. This correlation was obtained from systems of various Group A particles. It is seen that this correlation can fit the high solids circulation rate data very well, but this is not the case for low solids circulation rate. For both solids circulation rates, a uniform dilute zone is observed in the core region, which is followed by a pronounced decrease in voidage (or increase in solids

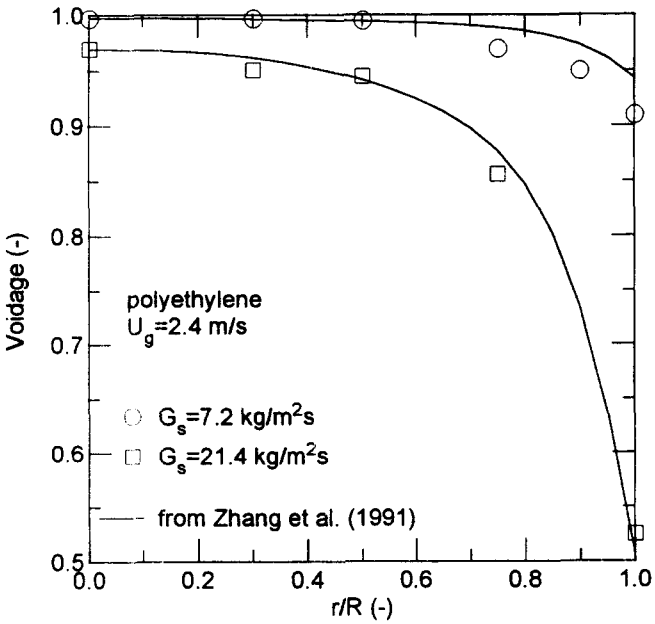

Figure 7. Time-averaged radial distribution of the voidage.

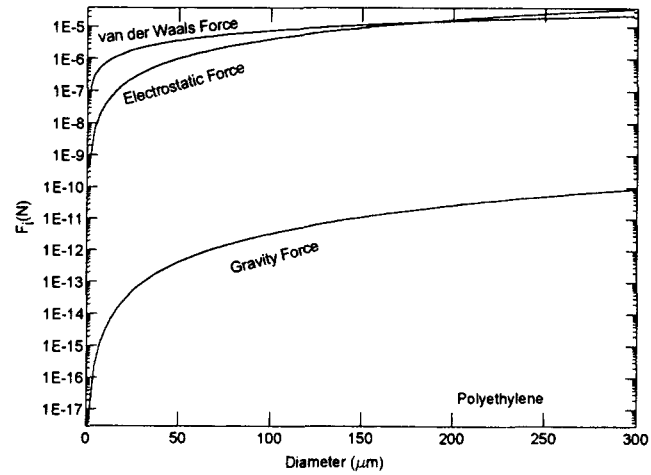

Figure 8. Theoretical estimation of van der Waals forces and electrostatic forces for polyethylene particles.

concentration) in the wall region. The small deviation of the voidage for polyethylene particles from that of common Group A particles in the dilute condition may be due to electrostatic attraction between the wall, or a dust layer adhered on the wall, and particles in bulk flow.

Interparticle forces for polyethylene particles

The particle physical properties affect the fluidization behavior in a circulating fluidized-bed system through the hydrodynamic forces and interparticle force. The different behavior observed with polyethylene particles from other Group A particles reflects the increased relative importance of the interparticle forces in comparison with the hydrodynamic or gravitational force. There are two main interparticle forces that can act in a circulating fluidized bed: van der Waals and electrostatic forces. It is generally agreed that the van der Waals forces are the dominating forces at particle-particle contact and are responsible for preserving formed agglomerates. On the other hand, electrostatic forces play an important role in bringing particles together since they act over a longer range than van der Waals forces. The theoretical estimate of van der Waals and electrostatic forces for polyethylene particles based on the equations given below is plotted in Figure 8. For comparison, the gravitational force is also given in this figure.

According to Krupp (1967), van der Waals force per particle contact is estimated by:

$$F_v \approx \frac{h\omega}{8\pi z_0^2} R\left(1 + \frac{h\omega}{8\pi^2 z_0^3 H_s}\right) \tag{1}$$

where $h\omega$ is the Lifschitz-van der Waals constant determined from dielectric spectra of the interaction material, z_0 is the separation distance at contact usually taken for solid as 4 Å (Krupp, 1967) and H_s is the hardness of the softer of the two spheres and takes into account the repulsive forces resisting surface deformation. Van der Waals force is affected by the surface geometry of the contacting particles, which is characterized by a parameter R. The presence of nodules on the surfaces of the PE particles will reduce the radii of curvature

at the contact points between particles compared to that for the particles with smooth surfaces. Thus, the calculation of van der Waals force for PE particles is based on the radii of the nodules on the surface, which are estimated from the SEM photos of the PE particles (see Figure 2).

Polyethylene particles are dielectrics and will become electrostatically charged through triboelectric effects (Wolny and Kazmierczak, 1989). A charged particle will experience a force of attraction due to its own electrostatic image. The existence of a surface charge on a particle gives rise to an electrostatic field which has a maximum intensity at the particle surface. Due to its random nature, particle charging cannot be predicted theoretically. However, one approach is to calculate a theoretical maximum charge which a particle can carry. The maximum charge which can be built up on a surface is limited by the breakdown strength of the surrounding fluid. In air, the electric breakdown potential is 3×10^6 V/m and the permittivity of air is 8.8×10^{-12}. By applying Gauss' law, an estimate of the maximum charge for a spherical particle can be obtained from (Cross, 1987):

$$q_{\max}=2.64\times10^{-5}(\pi d_p^2)p \tag{2}$$

where $p=3\epsilon_r/(\epsilon_r+2)$ and ϵ_r is the relative permittivity or dielectric constant of the material. Since the electrostatic force acting on a particle of charge, q, in an electric field E_e is given by $F_e=E_eq$, the maximum electrostatic force at the condition of incipient breakdown in air is:

$$Fe_{\max}=248.8d_p^2p \tag{3}$$

Therefore, calculating the maximum electrostatic force as a function of particle diameter requires only the knowledge of the static dielectric constant of material. Polyethylene particles have strong electrostatic forces due to large dielectric constant. Note that the assumption of the maximum charge can be justified by the fact that electric sparks can be observed frequently in the circulating fluidized bed (CFB) system.

The fluidization behavior of polyethylene depends on the combined effects of the van der Waals, electrostatic and hydrodynamic forces. As seen from Figure 8, electrostatic and van der Waals forces are both important for PE particles. Even for large PE particles, the electrostatic forces are still important attraction forces, unlike the common Group A particles. On the other hand, the importance of the interparticle forces can be expressed in terms of a ratio of particle drag forces to interparticle forces. From Molerus (1982), the average tensile force transmitted per particle in a bed of voidage ϵ can be expressed as $F_i\pi/6\epsilon$, where F_i is the interparticle forces due to a single contact between two adjacent particles. If a one-dimensional fully developed flow is assumed, the drag force on a particle should balance its weight minus buoyancy, that is, $F_d=\pi d_p^3(\rho_s-\rho_g)g/6$. A much smaller ratio of drag forces to interparticle forces is obtained for PE particles ($\approx6.5\times10^{-4}$ for PE with a particle diameter of 100 μm and $\epsilon=0.95$) than that for common Group A particles. Large electrostatic forces have a two-fold impact on the fluidization behavior. At first, the fine fractions of PE particles adhere readily to the reactor wall, and a dust layer on the wall is observed all the time. Thus, the interactions between fluid or particles and the wall will change significantly. Secondly, for systems with high interparticle forces, particles cannot loosen up readily from their packing state, increasing the effective particle size.

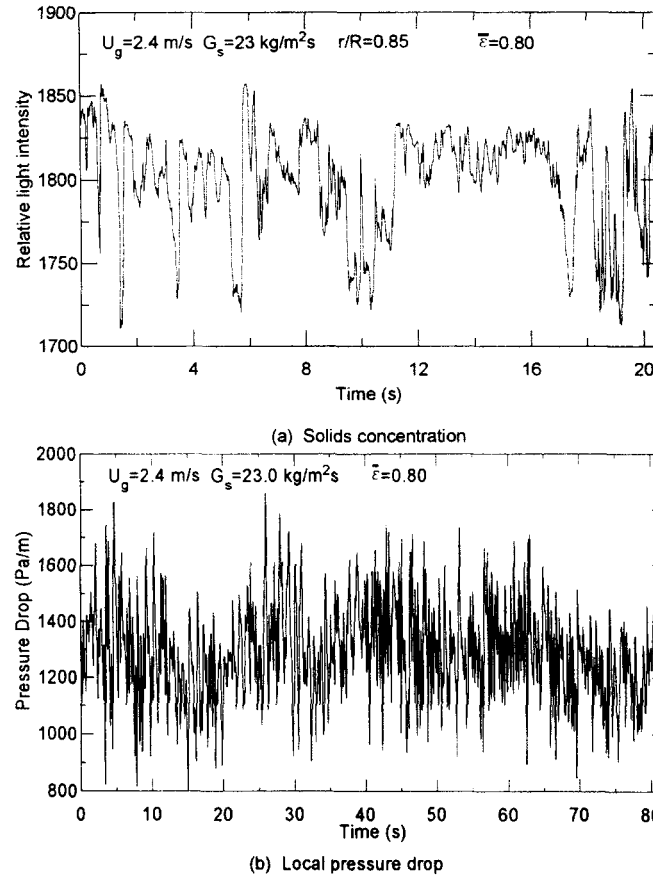

Figure 9. Typical pressure drop and solids concentration fluctuations measured in the dense condition.

Although the interparticle forces play an important role in characterizing the fluidization behavior of polyethylene particles, it is not possible to quantitatively analyze these forces in the gas-solid flow in the riser. The analysis described earlier is used qualitatively to explain the experimental observation in this study.

Flow structure

The flow structure for PE particles is analyzed through a statistical analysis of the instantaneous pressure drop and solids concentration reflected by the optic fiber probe signal. Figure 9 shows a typical example of these signals measured at the bottom dense region. At a low solids circulation rate, the pressure drop fluctuations are very random and a unimodal probability density function (PDF) with a sharp peak near the dilute side is observed (see $G_s=2.3$ kg/m^2·s in Figure 10a). With an increase in the solids circulation rate, the signals are characterized by fluctuations with multiple orders of temporal magnitude (aperiodic structure), and the peak in the PDF curve of pressure drop shifts to the high solids concentration side (see $G_s=19.6$ kg/m^2·s in Figure 10a). The similar trend of PDF has been reported by various investigators (for example, Schnitzlein and Weinstein, 1988) for common Group A par-

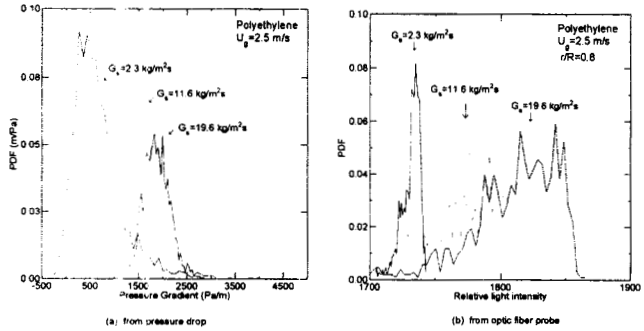

Figure 10. Probability density function of the local solids concentration at various solids circulation rates.

ticles. The PDF of local solids concentration shows a trend similar to that of the pressure drop in the case of a low solids circulation rate (see Figure 10b). A broad profile of the PDF for local solids concentration with a peak shifted towards the high solids concentration side is observed in the cases of high solids circulation rates. The variations of the PDF for both the pressure drop and local solids concentration also indicate that most fluctuations are distributed in a relatively narrow range on the high solids concentration side under conditions of high solids circulation rates. Note that bimodal PDF curves, representing the coexistence of particle clusters and individual particles in the local solids concentration measurement, have been reported for common Group A particles (Hartge et al., 1988).The absence of a bimodal distribution in the PDF of the pressure drop signals may result partially from the macro-measurement nature of the pressure drop (Weinstein et al., 1992). The skewness or lack of symmetry about the mean of the PDF of the local solids concentration signals increases with the solids circulation rate and eventually reaches a constant value. The skewness increases because the fraction of high solids concentration in the PDF increases due to the intermittent solid flow pattern. If it is assumed that the cluster exists in the measured zone when the voidage is less than 0.7, the presence/absence intermittency factor (time fraction of wall coverage by clusters) determined from the PDF of the local solids concentration acquired by the optic fiber probe is about 0.87 at the bottom dense region and $r/R=0.8$. This is slightly higher than the value of about 0.82 obtained from some data of Hartge et al. (1988) at the wall region for FCC particles. Wu et al. (1991) observed that the time fraction of the wall coverage by the solid cluster depends on the density of solids suspension, which provides further evidence of intermittent solid flow pattern. Their quantitative results also suggest that the wall is covered by densely packed particles most of the time.

The measured fluctuations in the pressure drop in the circulating fluidized bed can be attributed to the behavior of the cluster (including cluster size and shape) and to the turbulence in the dispersed phase, because the differential pressure variation is coupled with the dynamics of voidage fluctuation throughout the entire flow field. In other words, the large variation of the voidage indicates the generation of high amplitude peaks in pressure drop which is predominantly governed by solid flow patterns, especially by the local solids concentration distribution. These fluctuations have low frequencies due to the relatively low cluster passage frequency across the measurement zone. Note that high frequency signals are also generated when the clusters pass through the measurement zone, because the flow surrounding the clusters is in a highly turbulent state; the high frequency signals are superimposed on the low frequency fluctuations. To distinguish regular fluctuations in seemingly noisy signals, spectral analysis is used in the present study.

A highly resolved spectral density estimate of the pressure drop fluctuation will reveal periodic components as sharp peaks, even when the periodicities are of relatively small intensity. A sharp peak in the power spectrum of sample data, however, may also represent narrow-band random data. These two cases can usually be distinguished from one another by repeating the power spectral density measurement with a finer resolution filter bandwidth. If the measured spectral peak represents a sine wave, the indicated bandwidth of the peak will always be equal to the bandwidth of the analyzer filter, no matter how narrow the filter is. Furthermore, the indicated spectral density will always increase in direct proportion to the reduction in filter bandwidth. This method of detection is possible only if the resolution bandwidth of the analysis is smaller than the bandwidth of the possible narrow-band random data. This procedure is used to distinguish the periodic components in this study and the finest bandwidth used is 0.012 Hz; the dominant frequencies in an empty bed and in the measuring system are about 15 Hz and 11 Hz, respectively.

When the bed is operated in the dilute region, the dominant frequency in the normalized power spectrum falls near zero. With increasing solids circulation rate, a broad band with well defined bimodal profiles, one near 1 Hz and the other near 2.8 Hz identified with arrows in Figures 11b and c, is observed in the dense region. A typical normalized power spectral density function of the pressure drop signals recorded at 0.5–0.63 m above the distributor is shown in Figure 11. Note that the trend of the power spectral density function of pressure drop does not change with solids circulation rate in the bottom dense region (see Figures 11b and c). It seems that the local solids concentration is the key parameter to the solids flow pattern in the dense region, and the local solids concentration is insensitive to the solids circulation rate in the dense region as shown in Figure 6b for polyethylene particles. This insensitivity to G_s can be reinforced by the finding of King (1989), who developed an equation for the voidage in the dense region in which only U_g is involved (also see the section on solids holdup distributions). The shape of the power spectral density function also indicates that the power of the pressure drop distributes in a relatively narrow range of the frequency around the peaks. It is inferred that the large-scale wavy structure in the wall region and relatively small-scale cluster in the core region are the main components. Implicit in the idea of such a double structure is the assumption that the large wavy particle assemblage should have a quasi-deterministic form and the small-scale cluster in the core region is universally the same from flow to flow. The pressure drop and its fluctuations are determined overwhelmingly by the properties of the dense annular region, which is composed of partly stagnant or downwards flowing wave layer along the wall. The lack of sharp peaks in the power spectrum can be evidently attributed to the irregular variations of the wave layer and the cluster shape and size.

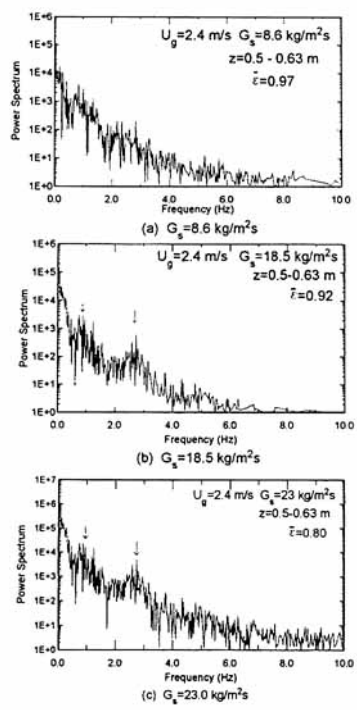

Figure 11. Power spectral density function of the pressure drop measured in the lower dense section.

The solid flow structure described above can also be used to interpret the experimental measurement of the radial voidage profile. There are two competitive factors affecting the radial solids concentration profiles: one is the drift of the particles towards the wall due to particle-particle interactions and electrostatic attraction; the other is the turbulent dispersion predominantly towards the core region, which may result in a more violent eruption of particles due to the relatively large-scale turbulent eddies generated under high solids concentration conditions. Referring to the radial voidage profile in the dilute conditions (see $G_s = 7.2$ kg/m^2·s in Figure 7), it may be inferred that particles diffused into the wall region tend to accumulate there where the gas velocity is low. However, the eddy in the wall region is not strong enough to eject all the particles back into the core region, thereby resulting in a higher solids concentration zone in the wall region. At high solids circulation rates, many particles are dispersed into the wall region, and consequently particle layers moving downward can be observed through the wall. Meanwhile, to maintain the solids circulating rate, the solids mass flux in the core region would have to increase in order to compensate for the reflux in the wall region, together with the simultaneous reduction of the effective flow area; this will increase the particle rising velocity in the core region. Strong hydrodynamic forces caused by the relative motion between the particle layer (downward) in the wall region and the stream of the gas-particle mixture (upward) in the core region will sweep the particle layer back into the core region. Under this condition, turbulent eddies generated by uneven distribution of solid particles become dominant. This can be confirmed by the variance of solids concentration, as shown in Figure 9a; large variation in solids concentration is observed in the wall region. When solids concentration is high, the particles swept into the core region will be diffused back into wall region due to strong particle interactions under high solids concentration conditions. Thus, a repeated solids flow pattern takes place in the wall region. This type of flow pattern has been uncovered by direct visual observation in this study. However, this flow structure cannot be seen in the time-averaged voidage profiles, because the time averaging filters out all dynamic characteristics.

Coarse particle effect on the bed of fine PE particles

Effects on the Operating Regime. For fine particles, the fluidization behavior is significantly affected by the interparticle forces. To improve the fluidization quality of PE particles, coarse particles are added to the bed of the fine PE particles. Collisions between fine particle clusters and coarse particles impede the formation of large clusters and hence improve operational stability. In Figure 4, the results of G_{tf} for the system with PE-CPE particle mixture (determined from operational instability consideration) are also shown. It is seen that G_{tf} is higher than that for a bed with fine PE particles alone at a given gas velocity, indicating that the fast fluidization regime can be achieved at higher solids circulation rates. These results are consistent with that of Satija and Fan (1985). They found that the terminal velocity of coarse particles in the air-fine particle medium of a multisolid circulating fluidized bed is lower than that in the air medium alone and it monotonically decreases with increasing fine particle flow rates. It is also observed that the fluidization quality is improved by the addition of coarse particles, as demonstrated by the reduction of the pressure drop fluctuations. Since the pressure fluctuation can be a good indication of gas-solid contact or solid particles distribution, the normalized fluctuation of pressure difference can be employed to characterize the fluidization quality in the present study.

Effect on Solids Concentration Profiles. Figure 12 shows typical apparent bed density axial profiles in the riser in the presence of coarse polyethylene particles (CPE). At a low gas velocity and a low solids circulation rate, coarse particles are retained in the bottom section of the bed and behave as a fixed bed. This is reflected in the axial profiles which exhibit a very dense region at the bottom section containing coarse and fine particles, and a dilute region at the upper section containing only fine particles (see ρ_m at $G_s = 7.4$ kg/m^2·s in Figure 12). With an increase in the solids circulation rate, coarse particles are entrained by the gas and fine particle stream and eventually carried out of the riser even though the gas velocity is lower than the single particle terminal velocity of the coarse particles. Particle collisions are responsible for entrainment of coarse particles. The probability of collisions between coarse and fine particles will rise with an increase in the solids circulation rate. This increased interaction causes a momentum transfer from fast-moving fine particles to slow-moving coarse particles. At $G_s = 13.5$ kg/m^2·s in Figure 12 the axial variation of the apparent bed density becomes less pronounced and the apparent bed density at the entrance region of the bed is significantly lower compared to that at $G_s = 7.4$ kg/m^2·s. The fine particle circulation rate may reach the saturated carrying capacity and coarse particle concentrations become relatively dilute. Thus, fine particles are accumulated at the bottom region, resulting in an S-shaped apparent bed density profile (see ρ_m at $G_s = 13.5$

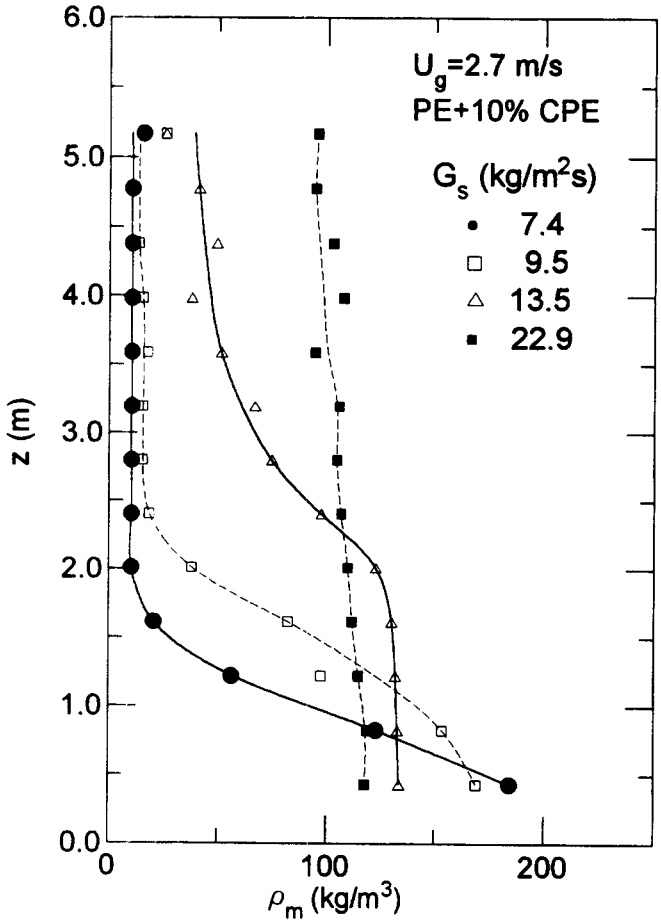

Figure 12. Typical apparent bed density axial profiles in the system with the presence of coarse particles.

kg/m^2·s in Figure 12). As the solids circulation rate is further increased, the apparent bed density at the bottom is further reduced, and the dense region extends to the exit of the riser (see ρ_m at G_s=22.9 kg/m^2·s in Figure 12). Note that coarse particles are not segregated when they participate in the circulation with fine particles. Similar observations were also made by Nowak et al. (1990) for a mixture of FCC and 3 mm porous silica alumina and by Bi et al. (1992) for the mixture of FCC and CPE particles.

Figure 13 gives a comparison of typical axial solids concentration profiles with and without coarse particles. It can be seen that at a low solids circulation rate, the solids holdup for the system with coarse particles is generally higher than that without coarse particles, especially at the bottom region where coarse particles remain. With increasing solids circulation rate, as a result of coarse particle recirculation, the solids holdup in the upper section will be significantly increased. Correspondingly, the solids holdup at the bottom section becomes a little lower than that without coarse particles (see ρ_m at G_s=20.8 kg/m^2·s in Figure 13a, and at G_s=22.9 kg/m^2·s in Figure 13b). An increase in the solids holdup in the upper region can also be attributed to the enhancement of interactions between fine and coarse particles.

Effect on Overall Fine Solids Holdup. Based on the as-

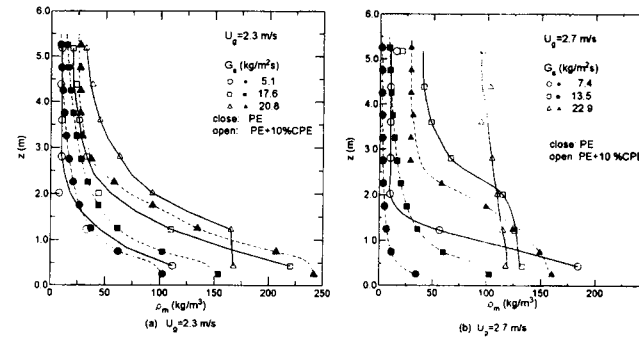

Figure 13. Effects of coarse particles on the apparent bed density axial profile.

sumption that the pressure drop equals the weight of the suspended particles, the overall fine solids holdup in the riser with coarse particles can be obtained as follows. The overall pressure drop across the bed can be expressed as:

$$\Delta P_{tcf} = (\rho_{sc}\bar{\epsilon}_{sc} + \rho_{sf}\bar{\epsilon}_{sf})gH \tag{4}$$

for system with both fine and coarse particles, and

$$\Delta P_{tc} = \rho_{sc}\bar{\epsilon}_{sc}gH \tag{5}$$

for system with coarse particles alone (that is, $\bar{\epsilon}_{sf}=0$). Solving Eqs. 4 and 5 for $\bar{\epsilon}_{sf}$ gives:

$$\bar{\epsilon}_{sf} = \frac{(\Delta P_{tcf} - \Delta P_{tc})}{\rho_{sf}gH} \tag{6}$$

As mentioned earlier, when the bed is operated at fairly low solids circulation rates and gas velocities, the coarse particles would remain in the riser. In this case, ΔP_{tc} can be obtained before the fine particles are circulated. On the other hand, when the riser is operated at relatively high solids circulation rates and/or gas velocities, a portion of the coarse particles are elutriated from the riser and recycled. Thus, the fraction of coarse particles confined to the riser would vary with the gas velocity and solids circulation rate. The overall pressure drop, ΔP_{tc}, in this case, can be obtained by shutting off all gas supplies to the riser and the L-valve, and elutriating all the fine particles from the bed.

The relationship between the solids circulation rate and the overall fine solids fraction for the systems with and without coarse particles is shown in Figure 14. Figure 14 shows that the fine solids holdup is significantly enhanced in the presence of coarse particles at both gas velocities shown, especially at the higher gas velocity. In an earlier study (Bi et al., 1992), it was found that for a gas velocity of 1.5 m/s, fine particle holdup is lower in the system with a combination of FCC and CPE particles than that in a bed of FCC alone. In contrast, at the gas velocity of 2.3 m/s the system with the CPE and FCC particles yields higher fine solids holdup. In the system with a combination of FCC and GB particles, however, increased fine solids holdup was observed at both gas velocities. In conjunction with the present results, it can be concluded that the critical solids circulation rate at which the coarse particles start being elutriated is strongly related to the en-

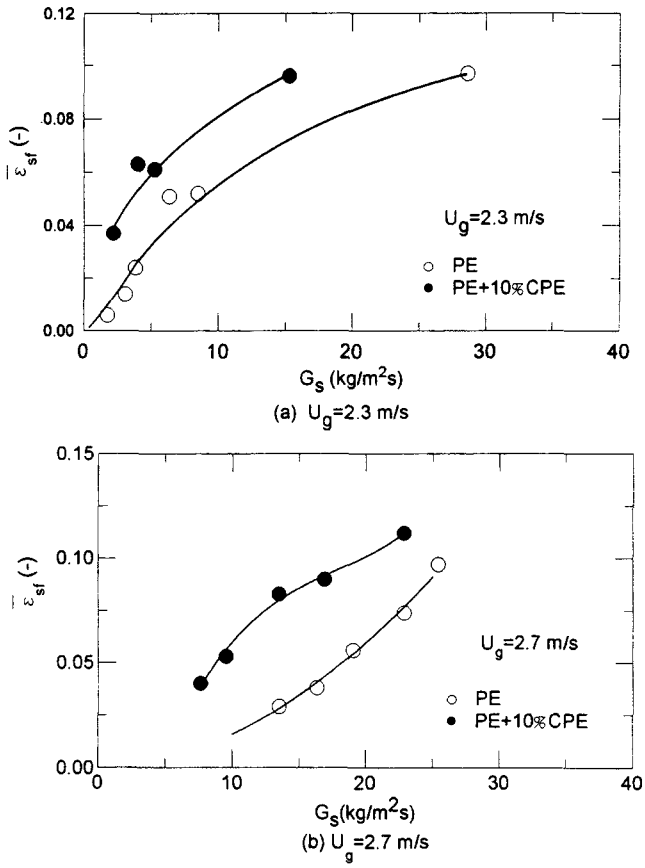

Figure 14. Effects of coarse particles on the overall fine polyethylene particle holdup.

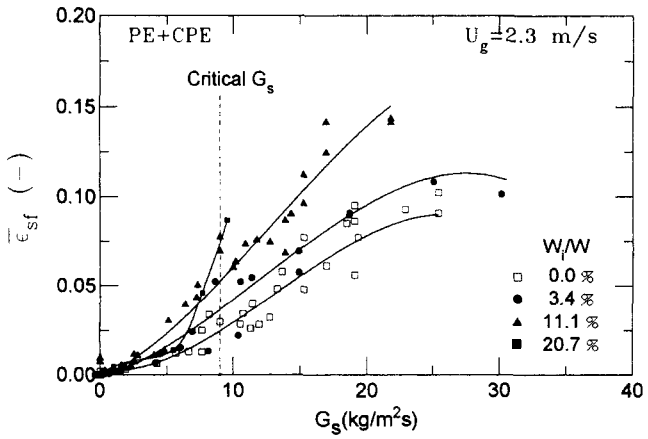

Figure 15. Effects of contents of coarse particles on the overall fine polyethylene particle holdup.

hancement of fine solids holdup because of the interactions between fine and coarse particles. According to Kitano et al. (1988), who examined the fine particle holdup in a fluidized dense bed of a multisolid pneumatic transport bed, this interaction force is proportional to the size of the coarse particles and inversely proportional to the size of the fine particles. The critical solids circulation rates at the gas velocity of 2.3 m/s are about 12, 4.5 and 8 kg/m^2·s for the systems of FCC-CPE, FCC-GB and PE-CPE, respectively. The critical solids circulation rate in the FCC-GB system is consistently the lowest among the three systems, and the effect of the coarse particles on the fine solids holdup is most pronounced. In contrast, the enhancement of the fine particle holdup is less significant for the FCC-CPE system, as reflected by a higher critical solids circulation rate.

There are two competitive factors affecting this enhancement in fine particles holdup. One is that the presence of coarse particles would slow down appreciably the movement of fine particles in the bed due to momentum interchange between coarse and fine particles through collisions, increasing the fine particle holdup. The other is due to the increase in interstitial gas velocity resulting from a decrease in the effective cross-sectional area of the flow because of the presence of coarse particles. The velocity of the fine particles would increase, causing the fine particle holdup to decrease. When the bed is operated at relatively low gas velocities, the coarse particles are retained in the bottom of the riser in a fluidized state. The probability of coarse-fine particle interaction is very small. In other words, the increase in the interstitial gas velocity dominates over the interactions between the fine and coarse particles. Thus, it would be expected that the fine particle holdup decreases or does not change significantly depending on the particle properties. At high gas velocities and high solids circulation rates with a large quantity of coarse particle presence, the large bed expansion of coarse particle yields large interactions between fine and coarse particles and hence high fine particle holdups.

Comparing the overall fine particle holdup in systems with different fractions of coarse particles in Figure 15, it is seen that a higher solids holdup can be achieved for systems with more coarse particles over the entire range of the coarse particles concentration studied. In addition, Figure 15 shows that the fraction of coarse particles contained in the system has little effect on the critical solids circulation rate (indicated by a vertical dash line in the figure), because the increase of coarse particles from 5 to 20 vol. % does not increase the static bed height significantly.

For the PE-CPE system, another factor contributing to the significant enhancement of fine particle holdup is the adhesion of fine particles on the surface of coarse particles at a low gas velocity. SEM analysis (see Figure 16) clearly shows that fine PE particles are adhered to the coarse particles, due to the electrostatic and van der Waals forces. The interparticle forces have a stronger effect than hydrodynamic forces for fine polyethylene particles at a low gas velocity (see Figure 8).

Simulated Momentum Exchange Between a Coarse Particle and a Cloud of Fine Particles. The fine particle holdup and the bed expansion of the coarse particles strongly depend on the momentum exchange between the coarse and fine particles through collisions, which in turn depends on the flow pattern and particle properties. For spherical particles in a circulating fluidized bed, it is reasonable to assume that the collisions are axisymmetric and torsionless. Therefore, for a collision between a coarse particle and a cloud of fine particles, the particle motion during the collision can be described by:

$$m_{sc}\frac{dU_{sc}}{dt} = F_{dc} + \eta F_{12} - F_{bc} \tag{7}$$

for a coarse particle. Here η is the number of fine particles

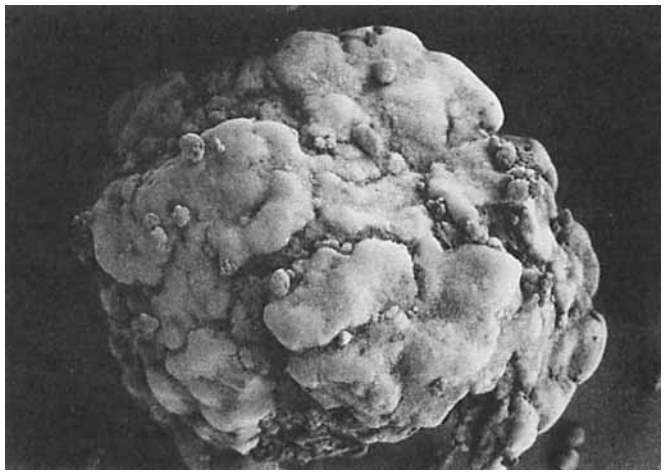

Figure 16. SEM photo showing the adhesion of fine particles on the surface of coarse particle for the PE-CPE system.

colliding simultaneously with the coarse particle in the direction of motion, and

$$m_{sf}\frac{dU_{sf}}{dt}=F_{df}-F_{12}-F_{bf} \tag{8}$$

for a fine particle. Combining Eqs. 7 and 8 yields the momentum transfer equation:

$$\frac{d}{dl}(U_{sf}-U_{sc})=-F_{12}\frac{m_{sc}+\eta m_{sf}}{m_{sc}m_{sf}}+\frac{F_{df}}{m_{sf}}-\frac{F_{dc}}{m_{sc}} \tag{9}$$

Note that in reaching the above equation it is assumed that both the coarse and fine particles experience the same body forces per unit mass. On the other hand, the change in the approaching distance between the coarse and the fine particles can be expressed as:

$$\frac{dl}{dt}=U_{sf}-U_{sc} \tag{10}$$

Substitution of $(U_{sf}-U_{sc})$ by Eq. 10 into Eq. 9 yields:

$$\frac{d^2l}{dt^2}=-F_{12}\frac{m_{sc}+\eta m_{sf}}{m_{sc}m_{sf}}+\frac{F_{df}}{m_{sf}}-\frac{F_{dc}}{m_{sc}} \tag{11}$$

Assuming the collisions to be elastic, based on Hertz theory of contact, the normal collision force can be expressed as (Goldsmith, 1960):

$$F_{12}=\frac{4}{3}E^*\sqrt{\frac{d^*}{2}}\,l^{\frac{3}{2}} \tag{12}$$

where

$$\frac{1}{E^*}=\frac{1-\nu_f^2}{E_f}+\frac{1-\nu_c^2}{E_c}\ \text{and}\ \frac{1}{d^*}=\frac{1}{d_{pf}}+\frac{1}{d_{pc}} \tag{13}$$

Substituting Eq. 12 into Eq. 11, rearranging the equation after multiplying dl/dt on both sides, and then integrating the equation with initial conditions:

$$\left(\frac{dl}{dt}\right)_{l=0}=U_{sf0}-U_{sc0}\ \text{and}\ l\,|_{t=0}=0 \tag{14}$$

yield

$$\frac{dl}{dt}=\sqrt{(U_{sf0}-U_{sc0})^2-\frac{16}{15}\frac{m_{sc}+\eta m_{sf}}{m_{sf}m_{sc}}E^*\sqrt{\frac{d^*}{2}}\,l^{\frac{5}{2}}+2l\left(\frac{F_{df}}{m_{sf}}-\frac{F_{dc}}{m_{sc}}\right)} \tag{15}$$

where U_{sf0} and U_{sc0} are particle velocities immediately before collision for fine and coarse particles, respectively. Note that the maximum compression occurs at the instant of zero relative velocity, that is, $dl/dt=0$. Hence, the maximum deformation, l_{max}, can be given by the solution of Eq. 15 by setting $dl/dt=0$, and the maximum collision force F_{12} can be obtained by substituting l_{max} into Eq. 12. Thus, the collision time can be determined by:

$$t_c=2\int_0^{l_{max}}\frac{dl}{\sqrt{(U_{sf0}-U_{sc0})^2-\frac{16}{15}\frac{m_{sc}+\eta m_{sf}}{m_{sf}m_{sc}}E^*\sqrt{\frac{d^*}{2}}\,l^{\frac{5}{2}}+2l\left(\frac{F_{df}}{m_{sf}}-\frac{F_{dc}}{m_{sc}}\right)}} \tag{16}$$

In a circulating fluidized bed, the coarse particles collide with a cloud of fine particles instead of a single particle. Only those fine particles whose centers lie within the cylindrical volume formed by the projected area $\pi(d_{pf}+d_{pc})^2/4$ and velocity vector $(U_{sf}-U_{sc})$ will collide with the coarse particle since the drag exerted by the surrounding gas can be balanced by the particle inertia. If a single scattering collision is assumed, the impact frequency can be expressed as:

$$f_c=\frac{\pi}{4}(d_{pf}+d_{pc})^2(U_{sf}-U_{sc})\bar{\epsilon}_{sf}/\frac{\pi}{6}d_{pf}^3 \tag{17}$$

Thus, the momentum exchange rate between the coarse and fine particles can be estimated through Eqs. 7, 12, 16 and 17.

The calculated results of the momentum exchange rate between a coarse particle and a cloud of fine particles due to collision for PE-CPE system are shown in Figure 17. In the model calculation, the drag forces on coarse and fine particles are estimated by (Bai et al., 1991):

$$\frac{C_D}{C_{DS}}=1.68\bar{\epsilon}^{0.253}\left(\frac{Re_r}{Re_t}\right)^{-1.213}\left(\frac{d_p}{D_c}\right)^{0.105} \tag{18}$$

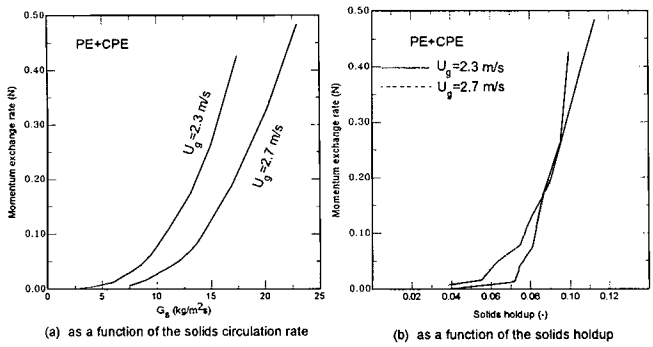

(a) as a function of the solids circulation rate (b) as a function of the solids holdup

Figure 17. Momentum exchange rate between a coarse particle and a cloud of fine particles due to collisions for the PE-CPE system.

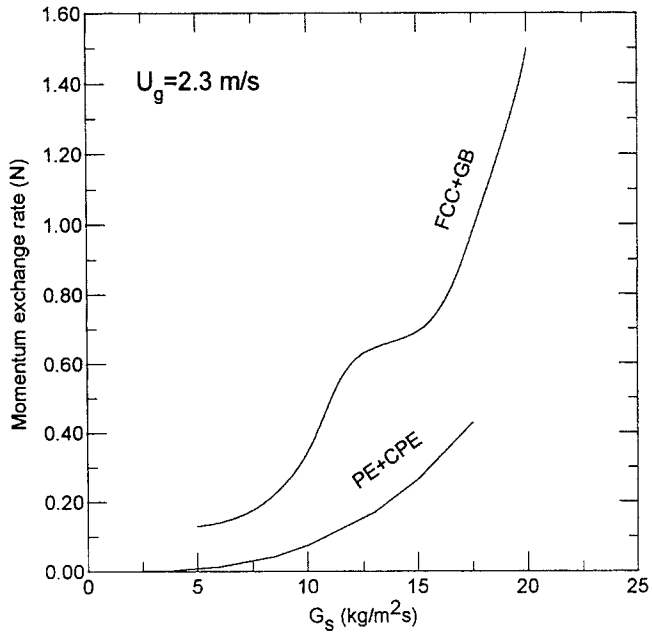

Figure 18. Comparison of the momentum exchange rate between a coarse particle and a cloud of fine particles in PE + CPE and FCC + GB systems.

where C_{DS} is the drag coefficient of a single particle in a uniform flow and can be evaluated by the following correlation (Clift et al., 1978):

$$C_{DS}=\frac{24}{Re_r}(1+0.15Re_r^{0.687}) \quad Re_r \le 800 \tag{19}$$

The gas and fine particle velocities are evaluated based on the assumption that the flow inside the riser is one-dimensional and steady. As discussed earlier, most coarse particles are in the suspension state in the operating range of the present study. It is therefore reasonable to assume that the coarse particle velocity is zero. Due to the extremely complex hydrodynamic behavior in a riser with polymer resin particles, solids holdup cannot be easily predicted theoretically; the experimentally measured solids holdups are thus used in the model calculation. The number of fine particles colliding with a coarse particle at any moment is approximated by the product of the number density of fine particles and the projected area of a coarse particle in the moving direction, that is, $\eta=\bar{\epsilon}_{sf}(d_{pc}^2/d_{pf})^3$. As can be seen in Figure 17, the momentum exchange rate increases with solids circulation rate for both gas velocities of 2.3 and 2.7 m/s; the increase is more pronounced at high solids circulation rates, which suggests a strong interaction between particles. These results support the experimental observations described earlier. During the particle collision, coarse particles gain momentum. As a result, coarse particles start to move away from the settling state even though the drag forces are not sufficient to lift up these coarse particles. When solids circulation rate is further increased, coarse particles participate in the circulation with the fine particles due to high momentum transfer rate, as shown in Figure 17a. On the other hand, the fast moving fine particles lose momentum during the collisions, and their velocity will be reduced significantly due to their smaller inertia. This is consistent with the measurements of fine particle holdups. Note that the momentum exchange rates are almost the same for both the gas velocities under the same solids holdup, as shown in Figure 17b. Comparing the results between the two gas velocities, it is found that the impact frequency is the dominant factor affecting the momentum exchange and hence the fine particle holdup. A comparison of the momentum exchange rate between the coarse particle and fine particles in the PE + CPE and FCC + GB systems are shown in Figure 18. The higher momentum exchange rate for the FCC + GB system is in good agreement with the higher enhancement of fine particles holdup.

Concluding Remarks

The hydrodynamic behavior of a circulating fluidized bed using polyethylene resins is systematically examined. The results indicate that the circulating fluidized bed can be operated smoothly in the fast fluidization regime with polyethylene resins. The transport velocity and the range of the operating regime for fast fluidization for polyethylene particles are obtained. The flow structure is analyzed based on pressure drop and local solids concentration fluctuations. The deviation of the hydrodynamic behavior of polyethylene particles from that of the common Group A particles can be explained by considering the interparticle forces. The effects of the addition of coarse particles to the circulating fluidized bed of fine polyethylene particles on the fluidization behavior are also investigated. It is found that the fluidization quality of polyethylene particles can be significantly improved with coarse particle addition. An increase in the overall fine particle holdup is observed, and the increase is interpreted in terms of fine-coarse particles interaction and an increase in the interstitial gas velocity. A mechanistic model accounting for the momentum exchange between the coarse and fine particles through collisions is also proposed, and the results of the model simulation are consistent with the experimental data obtained for fine solids holdups.

Acknowledgment

The assistance of Ms. Rhonda Lee in the calculation of interparticle forces is gratefully acknowledged.

Notation

C_D = drag coefficient of single particle in a riser
C_{DS} = drag coefficient of single particle in a uniform infinite flow
d_p = particle diameter, m
d^* = parameter defined in Eq. 13
D_c = riser diameter, m
E = Young's modulus of elasticity for particle, N/m^2
E_g = electric field, V/m
E^* = contact modulus defined in Eq. 13
f_c = impact frequency
F_{12} = force exerted on particle due to coarse-fine particle collision, N
F_b = body force exerted on particle, N
F_d = drag exerted on particle by the surrounding gas, N
F_e = electrostatic force of attraction, N
Fe_{max} = maximum electrostatic force of attraction, N
F_i = interparticle forces, N
F_v = van der Waals force of attraction, N
g = acceleration due to gravity, m/s^2
G_{pt} = the minimum solids circulation rate in the fast fluidization regime, kg/m^2·s
G_s = solids circulation rate, kg/m^2·s
G_{tf} = the maximum solids circulation rate in the fast fluidization regime, kg/m^2·s
$h\omega$ = Lifschitz-van der Waals constant, eV
H = height of the riser, m
H_s = hardness of solid material, N/m^2
l = approaching distance between two colliding particles, m
l_{max} = maximum deformation due to particle collision, m
m_s = particle mass, kg
p = defined in Eq. 2
ΔP_1 = pressure drop measured in the bottom section of the riser, Pa/m
ΔP_2 = pressure drop measured in the upper section of the riser, Pa/m
ΔP_{tcf} = overall pressure drop through the riser with fine and coarse particles, Pa
ΔP_{tc} = overall pressure drop through the riser with coarse particles alone, Pa
$(-\Delta P/\Delta L)$ = pressure difference, Pa/m
q = electric charge, C
q_{max} = maximum electric charge, C
R = characteristic measure of surface asperities, m
r/R = radial ratio of the riser
Re_r = particle Reynolds number based on relative velocity
Re_t = particle Reynolds number based on terminal velocity
t_c = particle collision time, s
U_g = superficial gas velocity, m/s
U_{mf} = incipient fluidization velocity, m/s
U_s = particle velocity, m/s
$U_{sf0} - U_{sc0}$ = initial relative velocity between coarse and fine particles, m/s
U_t = particle terminal velocity, m/s
U_{tr} = transport velocity, m/s
W_f/W = volumetric fraction of coarse particles in the system
z = axial distance from the distributor of the riser, m
z_0 = $\cong 4\times 10^{-10}$, distance at which maximum of van der Waals force is observed, m

Greek letters

ϵ = overall voidage
$\bar{\epsilon}$ = time and cross-sectional averaged voidage
ϵ_r = dielectric constant at zero frequency
ϵ_s = cross-sectional average solids holdup
$\bar{\epsilon}_s$ = overall solids holdup
η = number of fine particles colliding with a coarse particle at any moment
ν = Poisson's ratio
ρ_b = bulk density of particles, kg/m^3
ρ_g = gas density, kg/m^3
ρ_m = $(\rho_{sc}\epsilon_{sc} + \rho_{sf}\epsilon_{sf})$, cross-sectional average bed density, kg/m^3
ρ_s = particle density, kg/m^3

Subscripts

c = coarse particle
f = fine particle

Literature Cited

Bagster, D. F., and A. W. Roberts, "The Effect of Large Particles on the Flow Properties of Powders," *Powder Technol.*, **43**, 11 (1985).

Bai, D., Y. Jin, and Z. Yu, "The Particle Acceleration and the Interaction between Gas and Solids in the Riser of Circulating Fluidized Beds," *Fluidization Science and Technology*, M. Kwauk and M. Hasatani, eds., Beijing, Science Press, p. 46 (1991).

Basu, P., *Circulating Fluidized Bed Technology*, Pergamon Press, New York (1986).

Basu, P., M. Horio, and M. Hasatani, *Circulating Fluidized Bed Technology III*, Pergamon Press, New York (1990).

Bi, H. T., "Heat Transfer in Fast Fluidized Beds," MS Thesis, Tsinghua University, Beijing (1988).

Bi, H. T., P. J. Jiang, R.-H. Jean, and L.-S. Fan, "Coarse Particle Effects in a Multi-Solid Circulating Fluidized Bed for Catalytic Reactions," *Chem. Eng. Sci.*, **47**, 3113 (1992).

Cartwright, P., S. Sampuran, and A. G. Bailey, IAS-IEEE Annual Meeting, San Francisco, p. 1162 (1982).

Chang, H., and M. Louge, "Fluid Dynamic Similarity of Circulating Fluidized Beds," *Powder Technol.*, **70**, 259 (1992).

Clark, N. N., and C. M. Atkinson, "Amplitude Reduction and Phase Lag in Fluidized-Bed Pressure Measurements," *Chem. Eng. Sci.*, **43**, 1547 (1988).

Clift, R., J. R. Grace, and M. E. Weber, *Bubbles, Drops, and Particles*, Academic Press, New York, p. 111 (1978).

Cross, J. A., *Electrostatics: Principles, Problems and Applications*, Chap. 2, IOP Publishing Ltd., England (1987).

Geldart, D., and D. J. Pope, "Interaction of Fine and Coarse Particles in the Freeboard of a Fluidized Bed," *Powder Technol.*, **34**, 95 (1983).

Goldsmith, W., *Impact: The Theory and Physical Behavior of Colliding Solids*, Chap. IV, Edward Arnold (Publisher) Ltd., London (1960).

Hartge, E. U., D. Rensner, and J. Werther, "Solids Concentration and Velocity Pattern in Circulating Fluidized Beds," *Circulating Fluidized Bed Technology II*, J. F. Large and P. Basu, eds., Pergamon Press, New York, p. 165 (1988).

Ijichi, K., Y. Nishiyama, Y. Tanaka, Y. Uemura, Y. Hatate, H. Mineo, and K. Yoshida, "Particle Behavior within a Riser in a Two-Component System of Circulating Fluidized Bed," *Proc. Asian Conf. on Fluidized-Bed and Three-Phase Reactors*, Taibei, p. 111 (1990).

King, D. F., "Estimation of Dense Bed Voidage in Fast and Slow Fluidized Beds of FCC Catalyst," *Fluidization VI*, J. R. Grace, L. W. Shemilt, and M. A. Bergougnou, eds., Engineering Foundation, New York, p. 1 (1989).

Kitano, K., K. D. Wisecarver, S. Satija, and L.-S. Fan, "Holdup of Fine Particles in the Fluidized Dense Bed of the Multisolid Pneumatic Transport Bed," *Ind. Eng. Chem. Res.*, **27**, 1259 (1988).

Krupp, H., "Particle Adhesion Theory and Experiment," *Adv. in Colloid and Interf. Sci.*, **1**, 111 (1967).

Kunii, D., and O. Levenspiel, *Fluidization Engineering*, Chap. 2, Butterworth-Heinemann, Boston, p. 34 (1991).

Large, J. F., and P. Basu, *Circulating Fluidized Bed Technology II*, Pergamon Press (1988).

Li, H., R. Legros, C. M. H. Brereton, J. R. Grace, and J. Chaouki, "Hydrodynamic Behaviors of Aerogel Powders in High-Velocity Fluidized Beds," *Powder Technol.*, **60**, 121 (1990).

Molerus, O., "Interpretation of Geldart's Type A, B, C and D Powders by Taking Into Account Interparticle Cohesion Forces," *Powder Technol.*, **33**, 81 (1982).

Nakamura, K., and C. E. Capes, "Vertical Pneumatic Conveying of Binary Particle Mixtures," *Fluidization Technology, Vol. II*, D. L.

Keairns, ed., Hemisphere Publishing Corporation, Washington, DC, p. 159 (1976).
Nowak, W., H. Mineo, R. Yamazaki, and K. Yoshida, "Behavior of Particles in a Circulating Fluidized Bed of a Mixture of Two Different Sized Particles," *Circulating Fluidized Bed Technology III*, P. Basu, M. Horio, and M. Hasatani, eds., p. 219, Pergamon Press, New York (1990).
Richardson, J. F., and M. McLeman, "Pneumatic Conveying: II. Solids Velocities and Pressure Gradients in a One-Inch Horizontal Pipe," *Trans. Instn. Chem. Engrs.*, **38**, 257 (1960).
Satija, S., and L.-S. Fan, "Terminal Velocity of Dense Particles in the Multisolid Pneumatic Transport Bed," *Chem. Eng. Sci.*, **40**, 259 (1985).
Schnitzlein, M. G., and H. Weinstein, "Flow Characterization in High-Velocity Fluidized Beds Using Pressure Fluctuations," *Chem. Eng. Sci.*, **43**, 2605 (1988).
Smeltzer, E. E., M. L. Weaver, and G. E. Klinzing, "Pressure Drop Losses Due to Electrostatic Generation in Pneumatic Transport," *Ind. Eng. Chem. Process Des. Dev.*, **21**, 390 (1982).
Takeuchi, H., T. Hirama, T. Chiba, J. Biswas, and L. S. Leung, "A Quantitative Definition and Flow Regime Diagram for Fast Fluidization," *Powder Technol.*, **47**, 195 (1986).
Weinstein, H., M. Meller, M.-J. Shao, and R. J. Parisi, "The Effect of Particle Density on Holdup in a Fast Fluidized Bed," *AIChE Symp. Ser.*, **80**, p. 52 (1984).
Weinstein, H., H. J. Feindt, L. Chen, and R. A. Graff, "The Measurement of Turbulence Quantitites in a High Velocity Fluidized Bed," *Fluidization VII*, O. E. Potter and D. J. Nicklin, eds., Engineering Foundation, New York, p. 305 (1992).
Wolny, A., and W. Kazmierczak, "Triboelectrification in Fluidized Bed of Polystyrene," *Chem. Eng. Sci.*, **44**, 2607 (1989).
Wolny, A., and I. Opalinski, "Electric Charge Neutralization by Addition of Fines to a Fluidized Bed Composed of Coarse Dielectric Particles," *J. Electrostatics*, **14**, 279 (1983).
Wu, R. L., C. J. Lim, J. R. Grace, and C. M. H. Brereton, "Instantaneous Local Heat Transfer and Hydrodynamics in a Circulating Fluidized Bed," *Int. J. Heat Mass Transf.*, **34**, 2019 (1991).
Yerushalmi, J., and N. T. Cankurt, "Further Studies of the Regimes of Fluidization," *Powder Technol.*, **24**, 187 (1979).
Zhang, W., Y. Tung, and F. Johnsson, "Radial Voidage Profiles in Fast Fluidized Beds of Different Diameters," *Chem. Eng. Sci.*, **46**, 3045 (1991).

Manuscript received Mar. 3, 1993, and revision received Jun. 18, 1993.